

Alma Mater Studiorum Università di Bologna  
Archivio istituzionale della ricerca

Application and comparison of semi-empirical models for performance prediction of a kW-size reciprocating piston expander

This is the final peer-reviewed author's accepted manuscript (postprint) of the following publication:

*Published Version:*

Bianchi M., Branchini L., De Pascale A., Melino F., Ottaviano S., Peretto A., et al. (2019). Application and comparison of semi-empirical models for performance prediction of a kW-size reciprocating piston expander. APPLIED ENERGY, 249, 143-156 [10.1016/j.apenergy.2019.04.070].

*Availability:*

This version is available at: <https://hdl.handle.net/11585/706126> since: 2020-02-12

*Published:*

DOI: <http://doi.org/10.1016/j.apenergy.2019.04.070>

*Terms of use:*

Some rights reserved. The terms and conditions for the reuse of this version of the manuscript are specified in the publishing policy. For all terms of use and more information see the publisher's website.

This item was downloaded from IRIS Università di Bologna (<https://cris.unibo.it/>).  
When citing, please refer to the published version.

(Article begins on next page)

This is the final peer-reviewed accepted manuscript of:

Michele Bianchi, Lisa Branchini, Andrea De Pascale, Francesco Melino, Saverio Ottaviano, Antonio Peretto, Noemi Torricelli,

Application and comparison of semi-empirical models for performance prediction of a kW-size reciprocating piston expander

*Applied Energy, Volume 249, 2019, pp. 143-156*

The final published version is available online at:

<https://doi.org/10.1016/j.apenergy.2019.04.070>

©2019. This manuscript version is made available under the Creative Commons Attribution-NonCommercial-NoDerivs (CC BY-NC-ND) 4.0 International License

(<http://creativecommons.org/licenses/by-nc-nd/4.0/>)

# Application and comparison of semi-empirical models for performance prediction of a kW-size reciprocating piston expander

M. Bianchi, L. Branchini\*, A. De Pascale, F. Melino, S. Ottaviano, A. Peretto, N. Torricelli

Alma Mater Studiorum, Università di Bologna - DIN, viale del Risorgimento 2, Bologna, 40136, Italy

\*corresponding author, e-mail: [lisa.branchini2@unibo.it](mailto:lisa.branchini2@unibo.it), phone: +39-051-2093314

## Abstract

This work presents the modeling and performance prediction of a prototypal reciprocating piston expander in the kW range of power. Two semi-empirical models have been selected from the literature and opportunely adapted to the case of study, then calibrated and validated over a full set of available experimental data. The first modelling approach is based on polynomial correlations of the expander efficiencies and it has been extended to account for the heat losses to ambient. The second one consists of a lumped parameters approach, that uses a few key geometrical data of the expander and some physical equations to describe the expansion process. The aim of this study is to detect the best approach, between those selected, for the simulation of reciprocating expander adopted in micro-scale ORC systems; this can provide a helpful tool for predicting the performance of machines in off-design conditions, not requiring detailed information on its internal geometry.

The calibration and validation procedures of the selected models have been performed thanks to an extensive experimental campaign on a test bench facility installed at the laboratory of the University of Bologna. Models comparison highlights that the lowest mean relative error value is obtained on the prediction of exhaust temperature, equal to 1 % and 2 % respectively for the polynomial and lumped model. Maximum relative errors are obtained in the prediction of rotational speed for the polynomial fitting model (equal to 10 %), and in the electric power output for the lumped approach (equal to 8 %). The global error function, calculated over the validation data set, is close to 5 % for both the applied modelling approaches.

Within the calibration range, the semi-empirical models show similar performance results of the output variables (i.e. electric power output, isentropic electric efficiency, rotational speed and filling factor). Conversely, when compared outside of the calibration range, prediction maps can substantially differ: the polynomial fitting functions model proves to be less accurate in the unexplored range of working conditions, overestimating the expander rotational speed while underestimating the value of the filling factor at high pressure ratios, and overestimating the isentropic electric efficiency values at low pressure ratios.

**Keywords:** reciprocating piston expander; modelling; semi-empirical models; calibration; validation; extrapolation capability; experimental data; Organic Rankine Cycle

## Nomenclature

<u>Symbols</u>	<u>Subscripts</u>
$A$ Area [m <sup>2</sup> ]	$0$ Clearance
$AU$ Overall heat transfer coefficient [W/K]	$actual$ Actual
$c_p$ Specific heat at constant pressure [J/kg/K]	$air$ Air
$D$ Diameter [m]	$amb$ Ambient
$FF$ Filling factor [-]	$calc$ Calculated
$GEF$ Global error function [-]	$calibrated$ Calibrated
$h$ Enthalpy [kJ/kg/K]	$comp$ Compression
$k$ thermal conductivity of the fluid [W/m/K]	$conv$ Conversion
$l$ Length [m]	$el$ Electric
$\dot{m}$ Mass flow rate [kg/s]	$ex$ Exhaust
$MRE$ Mean relative error [-]	$exp$ Expansion
$N$ Rotational speed [rpm]	$eq$ Equivalent
$NTU$ Number of transfer units [-]	$gen$ Generator
$n$ Number of samples [-]	$global$ Global
$Nu$ Nusselt number [-]	$in$ Inlet
$p$ Pressure [Pa]	$ins$ Insulating
$Pr$ Prandtl number [-]	$int$ Internal
$\dot{Q}$ Heat flow [W]	$is$ Isoentropic
$R$ Linear thermal resistance [m·K/W]	$leak$ Leakage
$Ra$ Rayleigh number [-]	$loss$ Loss
$Re$ Reynolds number [-]	$meas$ Measured
$r$ Radius [m]	$min$ Minimum
$r_v$ Volumetric ratio [-]	$pump$ Pump
$s$ Entropy [kJ/kg]	$recomp$ Recompression
$T$ Temperature [K] o [°C]	$ref$ Reference
$U$ Linear global heat transfer coefficient [W·m/K]	$sh$ Shaft
$u$ Velocity [m/s]	$su$ Supply
$V$ Volume [m <sup>3</sup> ]	$swept$ Swept
$v$ Specific volume [m <sup>3</sup> /kg]	$thr$ Throat
$\dot{W}$ Power [W]	$train$ Training
	$v$ Volumetric
	$val$ Validation
	$wall$ Wall
	$wf$ Working fluid
<u>Greek letters</u>	<u>Acronyms</u>
$\alpha$ Convective heat transfer coefficient [W/m <sup>2</sup> /K]	ct Constant
$\gamma$ heat capacity ratio [-]	HVAC & R Heating, ventilation, air conditioning & refrigeration
$\lambda$ Conductive heat transfer coefficient [W·m/K]	IV Independent variable
$\eta$ Efficiency [-]	L Level
$\rho$ Density [kg/m <sup>3</sup> ]	ORC Organic Rankine Cycle

## 1 Introduction

In a world where the energy demand is constantly increasing, the energy production sector must also face as soon as possible the emergency of the climate changes, reducing the global consumption of fossil fuels and the overall greenhouse gas emissions. This challenge can be accomplished by increasing the use of renewable energies, but also improving

1  
2  
3  
4 efficiency in conventional primary sources exploitation. In this context, also an efficient exploitation of small and micro-  
5 scale thermal sources, that are in general not valorized and thus wasted to the ambient – e.g.: low-value waste heat, low-  
6 enthalpy geothermal sources, solar thermal, biomass, etc. – can represent a substantial contribution for saving primary  
7 sources and emissions. The Organic Rankine Cycle (ORC) is currently recognized as one of the most efficient and flexible  
8 solution for converting low-grade heat into electricity, in small size systems [1]. Nevertheless, focusing on the micro range  
9 of power size (namely around 1-10 kW), the ORC technology is not mature and there are only few examples of early  
10 applications in the market [2].

11 The key component of micro-ORC systems is the expansion machine. The “state-of-the-art” micro-ORC expanders are  
12 mainly of positive displacement type, more suitable to be operated with low values of flow rate and expansion ratio and  
13 generally adopted when power output values are lower than 150 kW [3]. Among the different conceived expander  
14 technologies, there is not a prevailing solution for micro-ORC and there is still space for development in this dedicated  
15 research field. The cutting-edge architectures are scroll, screw, reciprocating and vane expanders; their design, in many  
16 cases, is derived from the compressors used in the HVAC & R industry. In some applications the same compressors are  
17 opportunely modified to operate in reverse mode. For example, Quoilin et al. [4] conducted an experimental and  
18 modelling study on a kW-size ORC system, working with a scroll expander derived from oil-free open-drive air compressor,  
19 while Ziviani et al. [5] characterized experimentally the performance of a single-screw air compressor converted to  
20 expander in a micro-ORC test bench, also mentioning the modifications implemented on the compressor seals, fluid ports  
21 and lubrication ports.

22 The selection of the proper expander architecture and design depends on several aspects, such as the heat source  
23 temperature, the operating expansion ratio, and on additional requirements in terms of compactness, reliability, costs etc.  
24 [6].

25 Performance prediction of the expander is of utmost importance in a power cycle, as it significantly affects the overall  
26 system energy conversion efficiency. Moreover, when implementing an existing expander architecture in a new heat  
27 recovery application, it can be interesting to know how the machine will work in this specific condition, that can be  
28 different from the original design point considered by the expander manufacturer; in such cases, experimental data on the  
29 expander performance in the extended range of operation can be not always fully available.

30 In this context, the availability of models for performance prediction of the expansion process can help significantly to  
31 optimize the design and the operation strategy for the new application of prototypal machines, limiting the need of  
32 experiments and thus saving time and costs.

33 If complete information about the internal geometry of the expander are not accessible (especially when using  
34 prototypes), as all the geometrical details cannot be fully available, or they are known only by the manufacturer, “semi-  
35 empirical” models can be helpful in predicting the expander performance. Such models are based on a combination of  
36 statistical correlations on experimental data and physical equations describing the process. The semi-empirical models  
37 have the advantages to offer a good trade-off among the pure deterministic models and the empirical ones, in terms of  
38 simulation speed, calibration efforts, modelling accuracy and extrapolation capability.

39 This kind of approach has been widely applied to the compressors of refrigeration facilities: for example, Li [7] developed a  
40 simplified physical model for hermetic scroll and also reciprocating compressors, with the aim of predicting mass flow  
41 rate, absorbed power and discharge temperature, validating the results with experimental data collected from literature.  
42 Molinaroli et al. [8] introduced a semi-empirical model of a rolling piston compressor, designed for different applications  
43 and working with different refrigerants, validating the results with manufacturer data. D’amico et al. [9] presented a semi-  
44 empirical thermodynamic model of a displacement pump integrated into an ORC experimental unit, where the pump  
45 behavior at design and off-design conditions is modeled as a set of thermodynamic processes, whose main geometrical  
46 parameters are calibrated using experimental data.

47 As far as the expanders are concerned, many modelling studies are focused on scroll and screw expanders for ORC  
48 systems. For example, Lemort et al. [10] presented the results of an experimental study carried out on a prototype of an  
49 open-drive oil-free scroll expander integrated into an ORC working with refrigerant R132, in order to estimate the  
50 contribution of the different losses. In the study of Ziviani et al. [11], the authors performed experimental tests on a 5 kW  
51 oil-free scroll expander working with R245fa, applying also a semi-empirical model in order to distinguish the different loss  
52 terms. Mendoza et al. [12] studied the performance of a scroll compressor modified to work as an expander, characterized  
53 by two different setups, using air and ammonia as working fluids. Giuffrida [13] proposed a modelling procedure in order  
54 to characterize the performance of a scroll expander for small ORC, when changing the working fluid. Ayachi et al. [14]  
55 investigated the performance of a hermetic scroll expander integrated into a Brayton cycle fed with R245fa. Giuffrida [15]  
56 improved the performance simulation of a single-screw expander, using different approach for modelling mechanical  
57  
58  
59  
60  
61  
62  
63  
64  
65

losses and ambient heat losses. A rotatory vane expander, for low to medium power output ORC applications, has been investigated by Vodicka et al. [16], in order to describe the loss term due to delayed contact of vane and stator. Regarding the reciprocating piston expanders, instead, the open literature is more limited. Among the few available studies, Glavatskaya et al. present and validate a steady-state simulation model for reciprocating piston expanders in [17], where the performance analysis of the expansion machine is carried out. Bouvier et al. [18] performed an experimental study on an oil-free piston expander working with water steam, developing also a semi-empirical model in order to conduct a sensitivity analysis for improving the control strategy.

## 1.1 Contribution and structure of the paper

In this paper, two semi-empirical literature models (the model by Li [7], originally introduced for compressors, and the model by Glavatskaya [17], for expanders) are elaborated, further extended and used for the case of a reciprocating expander prototype of a micro-ORC, which has been experimentally characterized with a dedicated test bench; the tests rough data used here as reference can be found in a previous study of the Authors [19].

The main contributions of this work can be summarized in: (i) a more detailed use of the two different models, with respect to the previous introduction, for the specific case of reciprocating piston expander and calibration for a prototype of kW-size, integrated into a micro-ORC system test bench facility for low grade heat recovery application; (ii) validation of the calibrated models with a different set of experimental data, over a wider range of operation; (iii) comparison of the calibrated models in predicting the piston expander behavior in an extrapolated range of operation, in order to understand potentialities and limitations and to obtain expander operating maps.

In paragraph 2, the two modelling approaches are presented, and the equations used to represent the expansion process are described. As innovative contribution, the Authors upgraded the first approach including a sub-model that calculates the heat losses to ambient, validating it by means of temperature sensors placed on the expander external surfaces. On the second selected model instead, with respect to the reference work [17], the terms related to the power losses have been rearranged, and also some of the parameters modified to better suit the specific application.

Paragraph 3 presents the calibration procedure and the validation process. The main features of the experimental facility used to collect the experimental data are briefly described.

Paragraph 4 shows and discusses the results of the validation procedure, reporting the mean relative errors on output variables and the global mean relative error. A final paragraph is dedicated to the extrapolation capability of the two models: the ability to predict the expander performance (i.e. power output, isentropic efficiency, filling factor and rotational speed) outside of the calibration data range is compared to identify the best modelling approach for this application.

## 2 Expander models

The two semi-empirical models considered in the study are here named as:

- 1) the “polynomial fitting functions model”, based on the work of Li [7];
- 2) the “lumped parameters model”, based on the work of Glavatskaya et al. [17].

These two models are applied here to a specific expansion machine; in particular, a reciprocating piston expander, consisting in three cylinders placed radially at 120°, with a total displacement equal to 230 cm<sup>3</sup> has been considered as test case. Figure 1 shows a schematic illustration of the machine architecture [20]. The expander geometry has been introduced in [21] and an experimental characterization is reported in [19], where the test bench specifics are also provided. The admission and discharge of the vapor at the expander are executed by rotary valves (details are not shown in Figure 1 for sake of simplicity), that are placed in correspondence of the cylinder head and are driven by the crankshaft rotation. The expander shaft is directly coupled to a three-phase electric generator in a hermetical sealed case, working at the same rotational speed. The expander is internally provided with a secondary passage (also not visible in figure) that is used to by-pass the cylinders in cold start-up operations, in order to let the fluid achieving the required superheating conditions and to warm up the expander casing to avoid thermal stresses. The external surface was insulated with a layer of mineral wool to reduce heat losses to the ambient, as visible in Figure 1 which shows the actual installation of the expander.

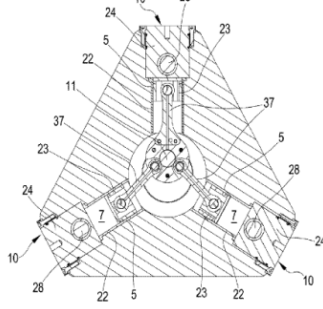
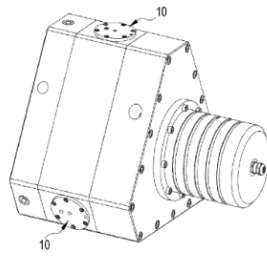


Figure 1. Piston expander prototype taken as reference for the models [20].

## 2.1 The polynomial fitting functions model

The polynomial fitting functions model was originally developed by Li [7] to simulate the performance of a volumetric compressor. The model is extended and applied here to model the reciprocating expander efficiency terms.

Figure 2 illustrates in detail the model scheme, which is based on simplified mass and energy balance equations. The main mass and energy flows that pass through the expander are shown in the figure. The model takes into account the supply inlet flow and the exhaust outlet flow (streams indicated as *su* and *ex* in Figure 2). The supply stream (with mass flow rate  $\dot{m}$ ) splits in two streams: the main one, with mass flow rate  $\dot{m}_{in}$ , undergoes the internal ideal expansion (black line in Figure 2); the leakage flow (green line in Figure 2), with mass flow rate  $\dot{m}_{leak}$ , by-passes the expansion process.

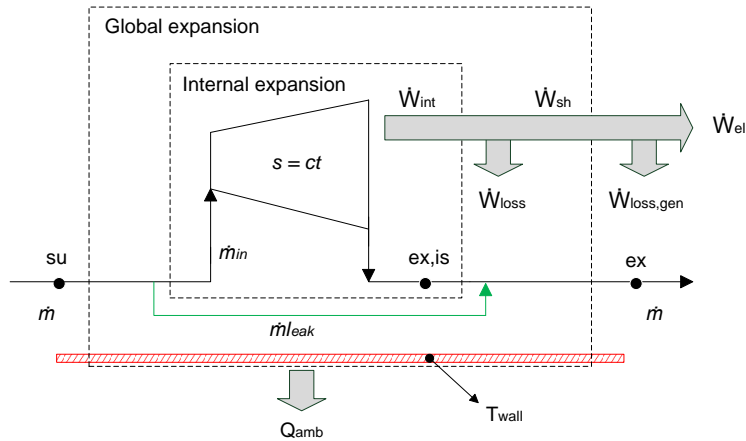


Figure 2. Polynomial fitting functions model scheme.

The input of the model are:

- the inlet mass flow rate ( $\dot{m}$ );
- the inlet or suction pressure ( $p_{su}$ );
- the inlet temperature ( $T_{su}$ );
- the outlet pressure ( $p_{ex}$ );
- the ambient temperature ( $T_{amb}$ ).

The main output quantities of the model are:

- the electric power output ( $\dot{W}_{el}$ );

- the rotational speed ( $N$ );
- the exit temperature ( $T_{ex}$ ).

Following the approach of the model by Li [7], the output quantities are calculated basically using two polynomial curves to represent the isentropic efficiency and the volumetric efficiency of the machine. In particular, the isentropic efficiency,  $\eta_{is}$ , can be expressed by a fitting polynomial equation (Eq. (1)), as function of the expansion pressure ratio  $\frac{p_{su}}{p_{ex}}$ :

$$\eta_{is} = a_2 \cdot \left(\frac{p_{su}}{p_{ex}}\right)^2 + a_1 \cdot \left(\frac{p_{su}}{p_{ex}}\right) + a_0 \quad (1)$$

where  $a_2$ ,  $a_1$ ,  $a_0$  represent empirical parameters to be calibrated by interpolation of experimental data. The volumetric efficiency,  $\eta_v$ , is also calculated through a polynomial function of the expansion pressure ratio:

$$\eta_v = b_2 \cdot \left(\frac{p_{su}}{p_{ex}}\right)^2 + b_1 \cdot \left(\frac{p_{su}}{p_{ex}}\right) + b_0 \quad (2)$$

where three additional empirical coefficients of interpolation  $b_2$ ,  $b_1$  e  $b_0$  are introduced.

The isentropic efficiency is used to calculate the shaft power ( $\dot{W}_{sh}$ ) and the electric power output; in particular, the shaft power is function of the isentropic power ( $\dot{W}_{is}$ ):

$$\dot{W}_{sh} = \dot{W}_{is} \cdot \eta_{is} \quad (3)$$

The electric power output depends on the shaft power and also on the generator electro-mechanical conversion efficiency ( $\eta_{conv}$ ) according to:

$$\dot{W}_{el} = \dot{W}_{sh} \cdot \eta_{conv} \quad (4)$$

The isentropic power in Eq. (3) can be calculated, with reference to the expander inlet mass flow rate, as:

$$\dot{W}_{is} = \dot{m} \cdot (h_{su} - h_{ex,is}) \quad (5)$$

where  $h_{su}$  is the supply enthalpy and  $h_{ex,is}$  is the exhaust isentropic enthalpy, corresponding to the exhaust pressure,  $p_{ex}$  and the supply entropy,  $s_{su}$ :

$$h_{ex,is} = f(p_{ex}, s_{su}) \quad (6)$$

It must be highlighted that the isentropic efficiency used in Eq. (3) includes both the internal loss due to friction (thermo-mechanical conversion loss) and the loss due to the leakage, depending on the volumetric efficiency.

The volumetric efficiency is used to calculate the expander rotational speed ( $N$ ), using the following definition:

$$\eta_v = \frac{\dot{m}_{in} \cdot 60}{N \cdot V_s \cdot \rho_{su}} \quad (7)$$

where  $V_s$  is the expander internal displacement,  $\rho_{su}$  is the supply density and  $\dot{m}_{in}$  is the internal mass flow rate; the  $\dot{m}_{in}$  value can be derived by the balance equation Eq. (8), referring to the internal expansion process (see also Figure 2):

$$\dot{m}_{in} \cdot (h_{su} - h_{ex,is}) = \dot{W}_{int} = \dot{W}_{sh} + \dot{W}_{loss} \quad (8)$$

where  $\dot{W}_{int}$  is the internal ideal power (i.e., considering that the internal mass flow undergoes the isentropic process), equal to the sum of the shaft power and of the friction losses contribution ( $\dot{W}_{loss}$ ).

In particular,  $\dot{W}_{loss}$  is here considered equal to the heat transfer loss through the expander wall to the ambient ( $\dot{Q}_{amb}$  in Figure 2). The evaluation of this term is discussed in details in the following paragraph, dealing with the modeling of the heat exchanged with the ambient.



Finally, the exhaust temperature,  $T_{ex}$ , is calculated as thermodynamic function of the exhaust pressure and of the exhaust enthalpy,  $h_{ex}$ :

$$T_{ex} = f(p_{ex}, h_{ex}) \quad (9)$$

where  $h_{ex}$  is obtained by the global expansion energy balance, according to:

$$\dot{m} \cdot (h_{su} - h_{ex}) = \dot{W}_{sh} + \dot{Q}_{amb} \quad (10)$$

#### 2.1.1 Calculation of the heat loss to ambient

For a comprehensive representation of the expansion process, a sub-model is included into the polynomial approach to calculate the heat loss to ambient ( $\dot{Q}_{amb}$  in Figure 2). The heat transfer term to the ambient is evaluated as:

$$\dot{Q}_{amb} = U \cdot l \cdot (T_{wf} - T_{air}) \quad (11)$$

where  $U$  is the equivalent linear heat transfer coefficient,  $l$  the equivalent length,  $T_{wf}$  the equivalent temperature of the working fluid inside the wall of the expander and  $T_{air}$  the external air temperature.

The  $U$  term and the temperature  $T_{wf}$  are calculated considering an equivalent expander geometry based on a simple model; in particular, the original geometry of the expander (visible in Figure 1) is approximated to a cylindrical element, with a circular cross section, as shown in Figure 3.

The  $l$  term represents the equivalent height of the cylinder, where  $l$  is calculated so that the overall heat transfer equivalent surface is equal to the total external surface of the real geometry. In this way  $l$  considers the heat exchange contribution both through the lateral walls and through the top and lower triangular faces.

As illustrated in Figure 3, the model considers three equivalent layers: the internal fluid, the expander wall and the external insulating layer; these layers correspond to the main domains of the actual expander geometry. The external radius of the three layers are indicated in figure as  $r_1$ ,  $r_2$  and  $r_3$ . The radius values of the equivalent layers are estimated on the basis of few external geometrical sizes of the machine. It must be observed that the proposed approach can be applied also to different external geometries for which not all the internal geometrical details are known.

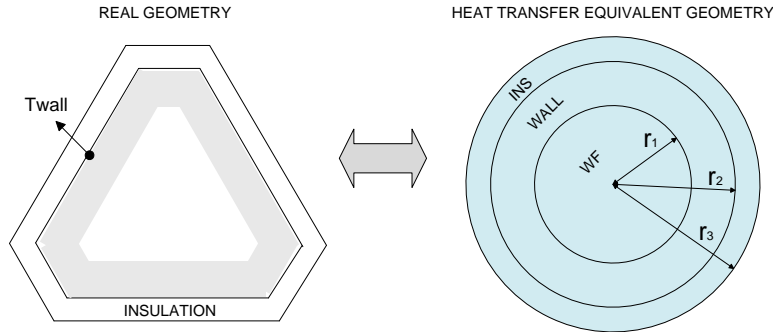


Figure 3. Cross section of the equivalent geometry of the heat transfer model.

The radius  $r_2$  is calculated using the actual external size of the expander (which can be easily measured) and considering an equal external perimeter. The value of  $r_3$  is obtained using the actual thickness of the insulating layer, as thickness of the annular external layer. The internal radius,  $r_1$ , is calculated assuming the corresponding internal volume equal to the expander internal displacement volume.

Then, the equivalent heat transfer coefficient,  $U$ , is calculated as:

$$U = 1/R_{global} \quad (12)$$

where the global thermal resistance  $R_{global}$ , is expressed as:

$$R_{global} = R_{wf} + R_{wall} + R_{ins} + R_{air} \quad (13)$$

where four resistance terms are introduced, namely the convective resistance of the air,  $R_{air}$ , the conductivity resistance of the wall material,  $R_{wall}$ , the conductivity resistance of the insulation,  $R_{ins}$ , and the convective resistance of the fluid,  $R_{wf}$ .

The resistance terms of each layer can be calculated using Eq.s (14-17):

$$R_{wf} = 1/(2 \cdot \pi \cdot r_1 \cdot \alpha_{wf}) \quad (14)$$

$$R_{wall} = \ln(r_2/r_1)/(2 \cdot \pi \cdot \lambda_{wall}) \quad (15)$$

$$R_{ins} = \ln(r_3/r_2)/(2 \cdot \pi \cdot \lambda_{ins}) \quad (16)$$

$$R_{air} = 1/(2 \cdot \pi \cdot r_3 \cdot \alpha_{air}) \quad (17)$$

where  $\lambda_{wall}$  and  $\lambda_{ins}$  are the wall and insulation layers conduction heat transfer coefficients, depending on the materials, while  $\alpha_{air}$  and  $\alpha_{wf}$  are the convective heat transfer coefficients for the external air and the organic fluid.

These convection coefficients  $\alpha$  can be calculated through the Nusselt number ( $Nu$ ), according to:

$$\alpha = Nu \cdot k/D \quad (18)$$

where  $k$  is the thermal conductivity of the fluid,  $D$  the corresponding diameter and  $Nu$  is evaluated with two different correlations. In particular,  $Nu_{air}$  is calculated with a correlation assuming natural convection in air [22]:

$$Nu_{air} = 0.59 (Ra_{air})^{0.25} \quad (19)$$

where  $Ra_{air}$  is the fluid Rayleigh number.

The  $Nu_{wf}$  value for the organic fluid is calculated by means of an experimental correlation based on the Dittus-Boelter formula for turbulent flows [22]:

$$Nu_{wf} = C \cdot (Re_{wf})^a \cdot (Pr_{wf})^b \quad (20)$$

where  $a$ ,  $b$  and  $C$  are parameters to be calibrated over the experimental data. The Reynolds number  $Re_{wf}$  is calculated using the expander inlet flow conditions and the equivalent diameter  $2r_1$ . The calibration of the constants that appear into the Nusselt correlation, will compensate, in part, the error committed using a simplified geometry.

## 2.2 The lumped parameters model

The second modelling approach selected to represent the behavior of the reciprocating piston expander is proposed by Glavatskaya et al. in [17] and named here as "lumped parameters model".

The target output quantities of the model, and the used main input, are the same of the previous model. The approach and the structure of the model equations are instead different, since the lumped parameters model takes into account some key geometrical data of the expander and it introduces additional physical equations, to describe the expansion process, instead of empirical polynomial functions. Nevertheless, also this model introduces additional parameters to be calibrated versus experimental data.

According to this approach, summarized in Figure 4, the model accounts for the following thermodynamic steps of the working fluid during the expansion process:

- an adiabatic pressure drop through the supply valve ( $su-su,1$  in Figure 4);
- a cooling effect, due to the heat exchange between the fluid and the wall at the suction side ( $su,1-su,2$ );
- an internal expansion process, modeled as an isentropic (2-3) plus a constant volume (3-4) transformation;
- a partial re-compression of the residual mass of the working fluid trapped into the clearance volume, which undergoes an isentropic (5-6) plus a constant volume (6-1) transformation;
- an adiabatic pressure drop through the discharge valve ( $ex,3-ex,2$ );
- a heat exchange effect between the wall and the fluid ( $ex,2-ex,1$ );

- a leakage effect of a fraction of the mass flow rate that by-passes the internal expansion ( $su,2-ex$ ).

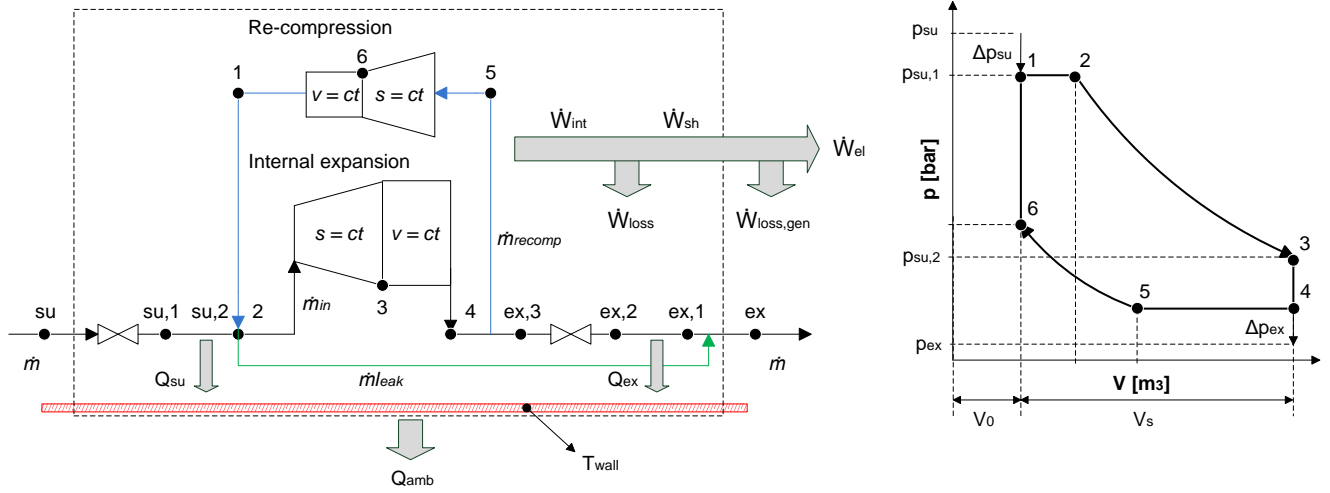


Figure 4. Lumped parameters model scheme and the respective p-V diagram representing the internal expansion process [17].

The main model physical equations are here briefly reported. The supply pressure drop between  $su$  and  $su,1$  is modelled as an isentropic expansion through a convergent nozzle, using the flowing equation:

$$\dot{m} = \rho_{su} \cdot A_{su} \cdot \sqrt{2 \cdot [h_{su} - h_{su,1}]} \quad (21)$$

where the model throat area  $A_{su}$  of the supply valve is a model parameter, to be identified by means of the calibration procedure, while  $h_{su,1}$  represents the calculated outlet enthalpy, used to obtain the exit pressure,  $p_{su,1}$ .

The leakage mass flow rate,  $\dot{m}_{leak}$ , is calculated, using an equation similar to Eq. (21), assuming an isentropic flow through a convergent nozzle, with a throat section area equal to the parameter  $A_{leak}$ ; in this case, the outlet enthalpy is evaluated with the throat critical pressure, assuming choking conditions, using the following equation:

$$p_{thr} = p_{su,2} \cdot \left( \frac{2}{\gamma_{su,2} + 1} \right)^{\frac{\gamma_{su,2}}{\gamma_{su,2} - 1}} \quad (22)$$

The heat exchanged at the supply section,  $\dot{Q}_{su}$ , required to calculate the fluid thermodynamic state in  $su,2$ , is obtained in this model by means of the NTU method, according to the following three equations:

$$\dot{Q}_{su} = \varepsilon \cdot c_p \cdot \dot{m} \cdot (T_{su,1} - T_{wall}) \quad (23)$$

$$\varepsilon = 1 - e^{-NTU} \quad (24)$$

$$NTU = \frac{1}{c_p \cdot \dot{m}} \cdot (AU)_{su,ref} \cdot \left( \frac{\dot{m}}{\dot{m}_{ref}} \right)^{0.8} \quad (25)$$

where  $\dot{m}_{ref}$  is the reference mass flow rate, evaluated in nominal operating conditions of the expander (assumed equal to 0.16 kg/s), while  $(AU)_{su,ref}$  is a calibration parameter of the model.

The expansion and the recompression transformations are modeled using the volumetric expansion ratio,  $r_{v,exp}$ , and the volumetric compression ratio,  $r_{v,comp}$ , respectively defined as (see Figure 4 for the fluid state numbering):

$$r_{v,exp} = \frac{V_3}{V_2} = \frac{v_3}{v_2} \quad (26)$$

$$r_{v,comp} = \frac{V_5}{V_0} = \frac{v_5}{v_6} \quad (27)$$

The two volumetric ratios are used to compute the fluid state at the end of the expansion process, after an isentropic and a subsequent isochoric transformation. The  $r_{v,exp}$  and  $r_{v,comp}$  parameters are here considered as unknown geometrical data, and they are obtained after calibration versus experimental data.

The mass flow rate that undergoes recompression,  $\dot{m}_{recomp}$ , responsible for a power loss contribution, is calculated as function of the clearance volume,  $V_0$ , according to:

$$\dot{m}_{recomp} = \frac{V_0 \cdot \rho_4 \cdot N}{60} \quad (28)$$

where  $V_0$  is a calibration parameter.

The expander shaft power,  $\dot{W}_{sh}$ , is expressed in the model including the expansion terms, the recompression term and the loss term, as:

$$\dot{W}_{sh} = \dot{m}_{in} \cdot (h_2 - h_4) - \dot{m}_{recomp} \cdot (h_1 - h_5) - \dot{W}_{loss} \quad (29)$$

where  $\dot{W}_{loss}$  represents the overall mechanical losses. This term is calculated in the model by accounting for two different contributes: a constant term,  $\dot{W}_{loss,ref}$  representing the constant mechanical loss and a second contribute,  $\dot{W}_{loss,N}$  proportional to the rotational speed:

$$\dot{W}_{loss} = \dot{W}_{loss,ref} + \dot{W}_{loss,N} \cdot N \quad (30)$$

The electric power,  $\dot{W}_{el}$ , is finally computed as:

$$\dot{W}_{el} = \dot{W}_{sh} \cdot \eta_{conv} \quad (31)$$

The rotational speed,  $N$ , is obtained as:

$$N = 60 \cdot \dot{m}_{in} / (\rho_2 \cdot V_2 - \rho_6 \cdot V_6) \quad (32)$$

The heat exchanged with the ambient,  $\dot{Q}_{amb}$ , is computed by Eq. (33), by means of the ambient heat transfer coefficient  $(AU)_{amb}$ .

$$\dot{Q}_{amb} = (AU)_{amb} \cdot (T_{wall} - T_{amb}) \quad (33)$$

where the wall temperature,  $T_{wall}$ , is calculated by the energy balance:

$$\dot{Q}_{amb} = \dot{Q}_{su} + \dot{W}_{loss} + \dot{Q}_{ex} \quad (34)$$

where the heat exchange at the exhaust section,  $\dot{Q}_{ex}$ , is described by means of the NTU method, with the nominal heat transfer coefficient  $(AU)_{ex,ref}$ , applying Eq.s (23-25), to the exhaust section  $ex,2$ .

The exhaust temperature can be finally obtained by the enthalpy mixing balance of the leakage stream and the expansion outlet stream.

### 2.3 Models parameters

Table 1 schematically resumes the considered key input and output variables, the constant quantities characteristic of the expander in study and the parameters of the two models that need to be found out through the calibration procedure.

In both the modeling approaches, the inlet stream conditions ( $T_{su}$ ,  $p_{su}$  and  $\dot{m}$ ), the outlet pressure ( $p_{ex}$ ) and the ambient temperature ( $T_{amb}$ ) are input data, representing the key boundary conditions of the expander operation. These inputs correspond to the independent values manipulated during the experimental tests on the machine. The swept or

displacement volume ( $V_s$ ), represents the main size fixed data of the machine; the nominal electric generator efficiency ( $\eta_{conv}$ ) value is provided by the electric generator manufacturer, and it has been considered constant and equal to 90 %. The polynomial fitting functions model requires as parameters to be calibrated the interpolation coefficients of the isentropic ( $a_0, a_1, a_2$ ) and volumetric efficiency functions ( $b_0, b_1, b_2$ ) and the coefficients of the Nusselt correlation ( $a, b, C$ ), used for the heat transfer sub-model.

The lumped parameters model, based on physical equations, is also characterized by physical calibration parameters, namely the heat transfer coefficients ( $(AU)_{su,ref}$ ,  $(AU)_{ex,ref}$  and  $(AU)_{amb}$ ), the friction losses coefficients ( $W_{loss,ref}$ ,  $W_{loss,N}$ ), the equivalent cross sectional areas ( $A_{leak}$ ,  $A_{su}$ ), the volume ratio coefficients ( $r_{v,exp}$ ,  $r_{v,comp}$ ) and the clearance volume ( $V_0$ ). It must be observed that in the second model case, the last three parameters are geometrical data that could be available if the expander internal design was completely known before the model application. Since for the prototypal case study under investigation these parameters were not known, they have been included among the calibration parameters set.

It has to be pointed out that the larger is the number of calibration parameters accounted into the model, the higher is the number of experimental data to consider, the higher is the computational cost of calibration, and the more difficult is to obtain an accurate calibration process.

Table 1. Summary of the input, output, constant values and models calibration parameters.

Inputs	
$T_{su}, p_{su}, p_{ex}, T_{amb}, \dot{m}$	
Constants	
$V_s = 230 \text{ cm}^3, \eta_{conv} = 90 \%$	
Model parameters	
“polynomial fitting functions model”	“lumped parameters model”
$a_2$	$(AU)_{su,ref}$ Supply heat transfer coefficient
$a_1$	$(AU)_{ex,ref}$ Exhaust heat transfer coefficient
$a_0$	$(AU)_{amb}$ Ambient heat transfer coefficient
$b_2$	$W_{loss,ref}$ Constant friction losses
$b_1$	$W_{loss,N}$ Proportional friction losses
$b_0$	$A_{leak}$ Equivalent leakage area
$a$	$A_{su}$ Supply nozzle equivalent section
$b$	$r_{v,exp}$ Expansion volume ratio
$C$	$r_{v,comp}$ Re-compression volume ratio
	$V_0$ Clearance volume
Outputs	
$T_{ex}, N, \dot{W}_{el}$	

### 3 Models calibration and validation

The upgraded models presented in paragraph 2 have been implemented in the MATLAB environment [23], along with a set of data coming from the experimental campaign. The working fluid thermo-fluid dynamic properties have been evaluated by means of REFPROP database [24]. In the following, the experimental setup and the procedures used for the calibration and validation of the models are described in detail.

#### 3.1 Experimental setup description

The prototypal reciprocating piston expander is integrated into a micro-ORC system test bench (in the kW range of power) [19]. The test bench is conceived for low grade heat recovery applications.

A simplified layout of the experimental facility is shown in Figure 5. It consists of a recuperated ORC using R134a as working fluid. The other components of the circuit are two brazed plate heat exchangers as evaporator and recuperator, a shell-and-tube condenser and a gear pump with frequency drive, that allows regulating the flow rate of the working fluid, since the pump is of positive displacement type.

The hot source is made by an electric water heater with rated power of 32 kW, that allows controlling the water temperature at the evaporator inlet between 50 °C and 100 °C, while as heat sink water well coupled with a compression chiller is used, providing a condenser inlet temperature variable between 13 °C and 28 °C. The test bench is fully equipped with an acquisition system, consisting in T-type thermocouples, absolute pressure transducers, flow meters and current and voltage transducers. In particular, the measured variables that are of interest for the model are the temperature and pressure at the inlet and outlet of the expander ( $T_{su}$ ,  $p_{su}$ ,  $T_{ex}$ ,  $p_{ex}$ ), the mass flow rate ( $\dot{m}$ ) acquired by the Coriolis flow meter at the pump suction point, the expander electric power output and rotating speed ( $\dot{W}_{el}$ ,  $N$ ), that are obtained by the electric transducers at the expander load terminals. Moreover, for the validation of the sub-model that accounts for heat losses to the ambient, two thermocouples have been positioned on the expander surfaces, one between the casing wall and the insulating layer and the other on the external surface of the insulator (see the detail of the expander in Figure 5).

The variables that can be controlled during the experiments are therefore the water temperature at the evaporator inlet ( $T_{H2O\ hot\ IN}$ ), the water temperature at the condenser inlet ( $T_{H2O\ cold\ IN}$ ) and the rotating speed of the feed pump ( $N_{pump}$ ). These control variables are directly related to the independent / input variables of the expander model, that are: i) the superheating temperature at the expander inlet ( $T_{su}$ ), determined by  $T_{H2O\ hot\ IN}$  (a quite constant and small difference between the  $T_{H2O\ hot\ IN}$  and  $T_{su}$  has been observed); ii) the organic fluid mass flow rate ( $\dot{m}$ ), affected by the pump speed; iii) the evaporation pressure ( $p_{su}$ ), which has a correlation with the flow rate of the working fluid and thus with the pump speed; iv) the condensation pressure ( $p_{ex}$ ), directly related to the condensing temperature which depends on cold water temperature.

The main features of the test bench components are reported in

Table 2, while further details (regarding also the acquisition system) can be found in [19].

The test campaign previously performed on the micro-ORC system provided a large amount of experimental data that can be used for the validation of the models; this data have been acquired in steady-state conditions, determined with the method described in [19]. Table 3 collects the range of variation of the main input variables considered in this work.

Finally, Figure 6 displays the experimental trends of supply and exhaust pressures and of the expansion ratio as function of the mass flow rate. The data shown in the figure are referred to tests conducted with a fixed value of cold water temperature (18 °C), to better highlight the influence of the working fluid flow rate on the system's pressures. Increasing the flow rate, a quasi-linear profile of the expander supply pressure is observed, while the exhaust pressure keeps barely constant, depending principally on the cold water temperature. Consequently, also the expansion ratio linearly increases with the flow rate, going from 1.8 to 2.7. Figure 6 is useful for defining the relation between the mass flow rate and the expander supply pressure: these two quantities indeed, are considered as independent input variables in the general description of the model (i.e. considering the expander by itself), but in the real operation of the system (i.e. with the expander included in the ORC circuit) they are correlated. Thus, when implementing the models to determine the performance maps, the supply pressure values are obtained from the mass flow rate input values, applying the equation corresponding to the red curve of Figure 6.

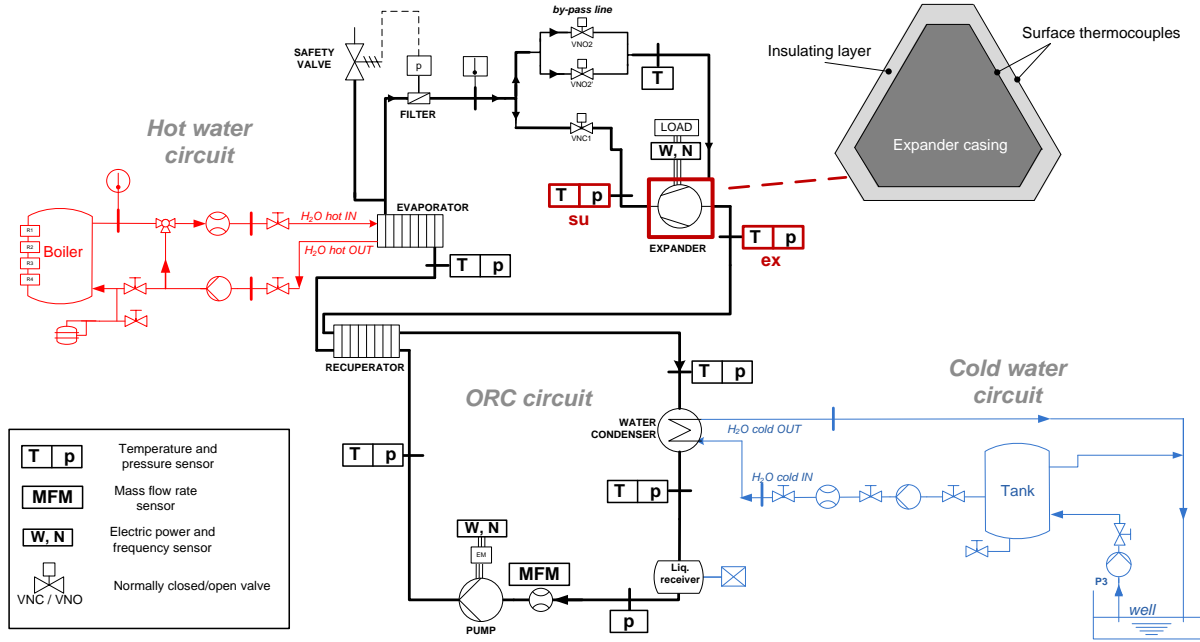


Figure 5. Layout of the micro-ORC experimental facility.

Table 2. Main features of the test bench components.

ORC circuit	
Heat exchangers	
Evaporator	brazed plate type
Recuperator	brazed plate type
Condenser	Shell and tube
Expander	
Architecture	3 radial reciprocating pistons
Total displacement	230 cm <sup>3</sup> /rev
Generator & load	3-phase permanent magnet generator + variable resistive load (3 kW max)
Feed pump	
Design	external gear pump
Motor	three phase motor

Hot water circuit	
Heat source	Electric water heater
Thermal input power range	8 – 32 kW
Water temperature	< 100°C
Water flow rate	1 – 2.6 l/s
Cold water circuit	
Cold sink	Water well (+ chiller)
Water temperature	13 – 28 °C
Water flow rate	1 – 2.8 l/s

Table 3. Range of measured data at steady state conditions

Input data range	
Supply temperature ( $T_{su}$ )	65 – 85 °C
Supply pressure ( $p_{su}$ )	10.9 – 20.5 bar
Working fluid mass flow rate ( $\dot{m}$ )	0.05 – 0.18 kg/s
Exhaust pressure ( $p_{ex}$ )	5.7 – 8.4 bar

Output data range	
Exhaust temperature ( $T_{ex}$ )	39.4 – 65.6 °C
Rotational speed ( $N$ )	319 – 898 rpm
Electric power ( $\dot{W}_{el}$ )	302 – 1356 W

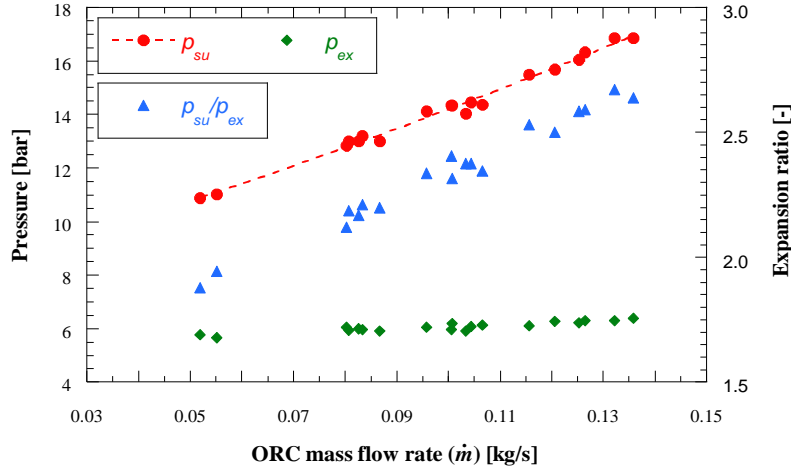


Figure 6. Experimental trends of supply pressure, discharge pressure and expansion ratio vs. working fluid mass flow rate.

### 3.2 Models calibration procedure

A schematic of the calibration procedure implemented in the MATLAB environment is summarized in Figure 7. The iterative procedure for models tuning allows determining the values of all the parameters listed in Table 1. As a common optimization problem, an initial value and a range of variation are necessary for each parameter to be determined. The calibration procedure ends as soon as the calculated models outputs agree with the experimental data within the error threshold.

For the calibration procedure, only a limited set of experimental data, called “training set”, have been used. As detailed in the following section, they represent a subset of the total available experimental data, which instead will be used for validating the extrapolation capability. This approach allows reducing the computational cost with a limited number of experimental data.

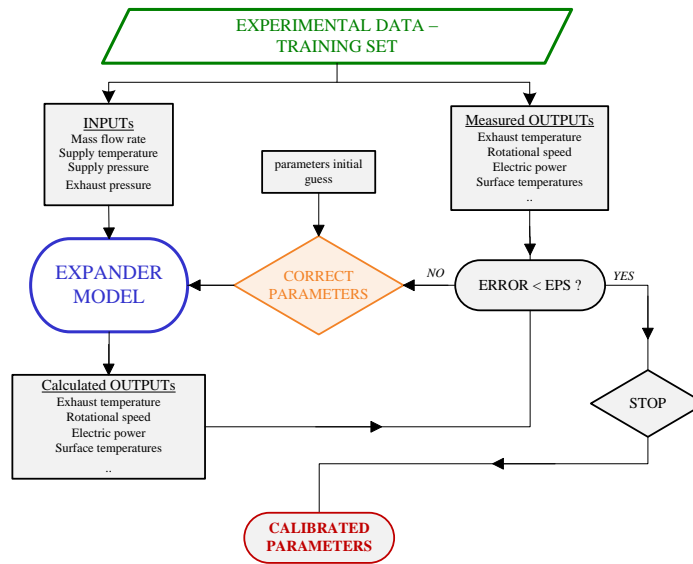


Figure 7. Schematic flow chart of the calibration procedure.

In the polynomial fitting model, the coefficients of the isentropic and the volumetric efficiencies equations (Eq.s (1) and (6) and Table 1) are obtained by interpolating the training data set with second degree functions. While, parameters used



into the Nusselt correlation (Eq. (20) and Table 1) to represent the heat exchanged with ambient, have been determined comparing model outputs and experimental results on two different surface temperatures.

In details, the wall temperatures considered are:  $T(r_2)$  - the temperature measured by a thermocouple placed between the steel wall and the insulating layer (see Figure 5)- and  $T(r_3)$  - the temperature measured by a thermocouple placed on the external surface of the insulating layer. The latter are calculated using the Eq.s (35-37)

$$T(r_1) = T_{wf} - (R_{wf}/l) \cdot \dot{Q}_{amb} \quad (35)$$

$$T(r_2) = T(r_1) - (R_{wall}/l) \cdot \dot{Q}_{amb} \quad (36)$$

$$T(r_3) = T(r_2) - (R_{ins}/l) \cdot \dot{Q}_{amb} \quad (37)$$

The lumped models parameters have been identified based on the minimization of a global error function (*GEF*) on the predictions of exhaust temperature, rotational speed and electric power output, defined as:

$$GEF = \frac{1}{3} \sqrt{\frac{1}{n_{train}} \sum_{i=1}^{n_{train}} \left( \frac{T_{ex,calc,i} - T_{ex,meas,i}}{T_{ex,calc,i}} \right)^2} + \frac{1}{3} \sqrt{\frac{1}{n_{train}} \sum_{i=1}^{n_{train}} \left( \frac{N_{calc,i} - N_{meas,i}}{N_{calc,i}} \right)^2} + \frac{1}{3} \sqrt{\frac{1}{n_{train}} \sum_{i=1}^{n_{train}} \left( \frac{\dot{W}_{el,calc,i} - \dot{W}_{el,meas,i}}{\dot{W}_{el,calc,i}} \right)^2} \quad (38)$$

where the function is evaluated over the training set data ( $n_{train}$ ).

The minimization process has been carried out by using a genetic algorithm routine, available in MATLAB Optimization Toolbox [25] and specifically dedicated to multivariable functions.

The choice of the “training set” among all the experimental data has been carried out by means of the matrix experiments, as reported in Table 4. The purpose is to select the most significant points included within a predetermined calibration range. The independent variables (IV columns in Table 4) controlled during the tests are: the supply temperature ( $T_{su}$  as IV1), the mass flow rate of the organic fluid entering the expander ( $\dot{m}$  as IV2) and the exhaust pressure ( $p_{ex}$  as IV3). Each independent variable assumes discrete values (indicated by L): three for the supply temperature (65 °C; 75 °C; 85 °C) and the mass flow rate (0.08 kg/s; 0.10 kg/s; 0.12 kg/s), two for the exhaust pressure (6 bar; 7 bar).

Therefore, cells of the matrix represent the eighteen possible combinations used for the calibration procedure.

Table 4. Matrix experiments for the training set selection.

			IV1 T <sub>su</sub> [°C]	IV2 ṁ [kg/s]	IV3 p <sub>ex</sub> [bar]
IV1-L1	IV2-L1	IV3-L1	65	0.08	6
	IV2-L1	IV3-L2	65	0.08	7
	IV2-L2	IV3-L1	65	0.10	6
	IV2-L2	IV3-L2	65	0.10	7
	IV2-L3	IV3-L1	65	0.12	6
	IV2-L3	IV3-L2	65	0.12	7
IV1-L2	IV2-L1	IV3-L1	75	0.08	6
	IV2-L1	IV3-L2	75	0.08	7
	IV2-L2	IV3-L1	75	0.10	6
	IV2-L2	IV3-L2	75	0.10	7
	IV2-L3	IV3-L1	75	0.12	6
	IV2-L3	IV3-L2	75	0.12	7
IV1-L3	IV2-L1	IV3-L1	85	0.08	6
	IV2-L1	IV3-L2	85	0.08	7
	IV2-L2	IV3-L1	85	0.10	6
	IV2-L2	IV3-L2	85	0.10	7
	IV2-L3	IV3-L1	85	0.12	6
	IV2-L3	IV3-L2	85	0.12	7

### 3.3 Models validation procedure

The models validation has been carried out making use of the total available experimental data. To prove the effectiveness of the models in predicting the output variables (exhaust temperature, rotational speed and electric power), mean relative errors (*MRE*) (Eq.s (39-41)) and global error function (*GEF<sub>val</sub>*) (Eq. (42)) have been quantified. The function used for validation, differently from the one used for the calibration process (Eq. (38)), is therefore estimated over the total available experimental data (*n<sub>val</sub>*).

$$MRE_{Tex} = \sqrt{\frac{1}{n_{val}} \sum_{i=1}^{n_{val}} \left( \frac{T_{ex,calc,i} - T_{ex,meas,i}}{T_{ex,calc,i}} \right)^2} \quad (39)$$

$$MRE_N = \sqrt{\frac{1}{n_{val}} \sum_{i=1}^{n_{val}} \left( \frac{N_{calc,i} - N_{meas,i}}{N_{calc,i}} \right)^2} \quad (40)$$

$$MRE_{\dot{W}_{el}} = \sqrt{\frac{1}{n_{val}} \sum_{i=1}^{n_{val}} \left( \frac{\dot{W}_{el,calc,i} - \dot{W}_{el,meas,i}}{\dot{W}_{el,calc,i}} \right)^2} \quad (41)$$

$$GEF_{val} = \frac{1}{3} \sqrt{\frac{1}{n_{val}} \sum_{i=1}^{n_{val}} \left( \frac{T_{ex,calc,i} - T_{ex,meas,i}}{T_{ex,calc,i}} \right)^2} + \frac{1}{3} \sqrt{\frac{1}{n_{val}} \sum_{i=1}^{n_{val}} \left( \frac{N_{calc,i} - N_{meas,i}}{N_{calc,i}} \right)^2} + \frac{1}{3} \sqrt{\frac{1}{n_{val}} \sum_{i=1}^{n_{val}} \left( \frac{\dot{W}_{el,calc,i} - \dot{W}_{el,meas,i}}{\dot{W}_{el,calc,i}} \right)^2} \quad (42)$$

## 4 Results and comparison

Results of the calibration process are included in Table 5 where the obtained values of the models parameters are shown. Optimization algorithm, if not correctly implemented, can return a local minimum of the objective function, instead of the global one. In order to verify the robustness of the genetic algorithm application to the lumped parameters approach and to investigate the influence of each parameter on the global error value, a sensitivity analysis has been carried out. The Figure 8 shows the response of the model to a variation of calibrated parameters in the range  $\pm 10\%$ . As highlighted in the figure, the minimum of the *GEF* is obtained with a null variation of the entire set of the calibrated parameters, thus demonstrating that the obtained parameters identify a global minimum of the objective function. In addition, from the figure, it can be observed that there is a high sensitivity of the model to the supply nozzle equivalent section ( $A_{su}$ ), the supply heat transfer coefficient ( $AU_{su,ref}$ ) and to the exhaust heat transfer coefficient ( $AU_{ex,ref}$ ).

Table 5. Parameters identified by the calibration process for the polynomial fitting model a), and the lumped parameters one b).

a)	Parameter	value	b)	parameter	value	unit
	$a_2$	-0.2078		$A_{su}$	1.47e-05	m <sup>2</sup>
	$a_1$	0.9380		$A_{leak}$	5.51e-06	m <sup>2</sup>
	$a_0$	-0.6149		$AU_{su,ref}$	5.65e-05	W/K
	$b_2$	-0.2906		$AU_{ex,ref}$	9.23e-05	W/K
	$b_1$	1.2297		$AU_{amb}$	0.96	W/K
	$b_0$	-0.9738		$r_{v,exp}$	1.459	-
	$a$	0.675		$r_{v,comp}$	1.25	-
	$b$	0.365		$V_0$	2.32e-08	m <sup>3</sup>
	$C$	0.0154		$W_{loss,ref}$	0.198	W
				$W_{loss,N}$	1.07e-05	W/min

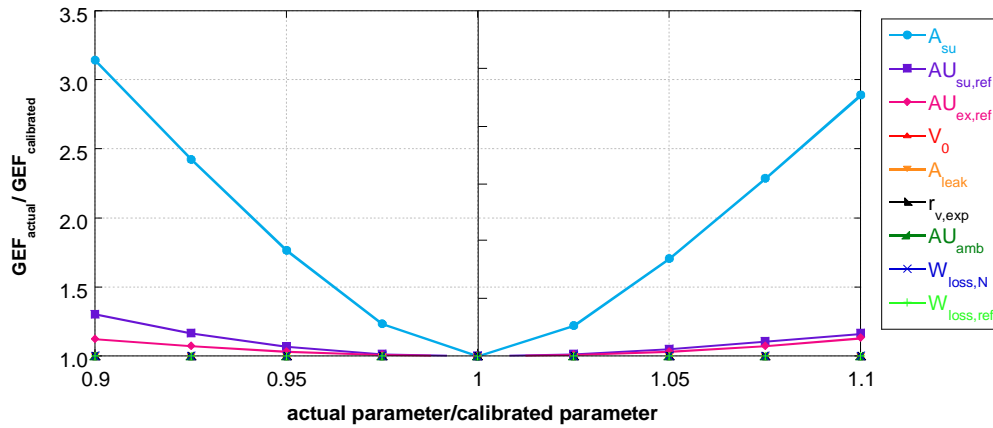


Figure 8. Sensitivity analysis of the GEF value to a variation of the calibration parameter value.

Figure 9 and Figure 10 focus on results of the validation procedure, respectively for the polynomial fitting and the lumped model approaches. The parity plots compare the calculated values of the output variables with the measured ones. In figures, the empty dots show the training set data.

The dash lines in figures highlight the mean relative error (Eq.s (39-41)) got on the output variables while exact values are shown in in Table 6 . Both models show the lowest *MRE* values on the prediction of exhaust temperature, equal to 1 % and 2 % respectively for the polynomial and lumped model (see Figure 9a and Figure 10a). Maximum relative errors are obtained in the prediction of rotational speed for the polynomial fitting model (equal to 10 % - see Figure 9b), and in the electric power output for the lumped approach (equal to 8 % - see Figure 10c).

The global mean relative error (Eq. (42)) obtained over the overall validation points, is close to 5 % for both the modelling approaches, thus proving that they are suitable to simulate the behavior of the reciprocating expander.

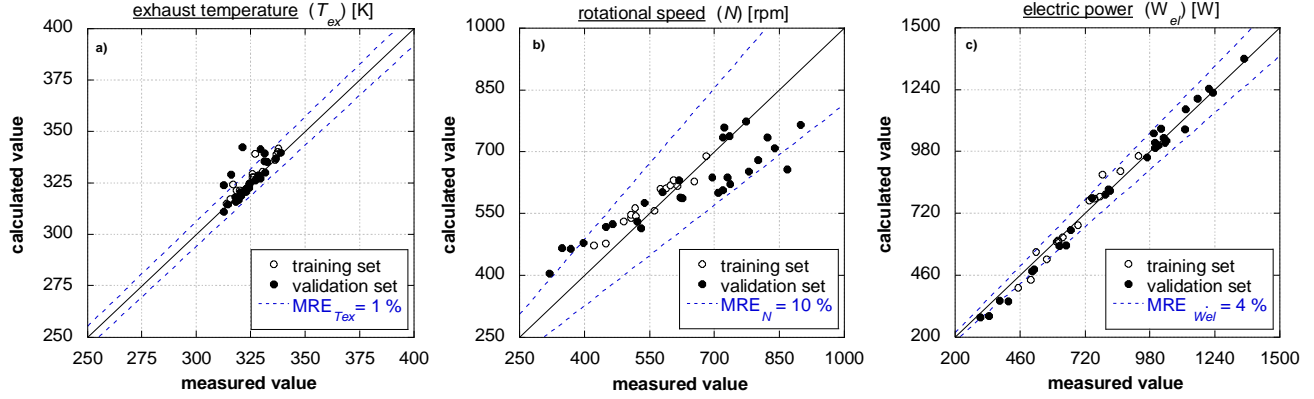


Figure 9. Parity plots of exhaust temperature a), rotational speed b) and electric power c) - polynomial fitting functions model.

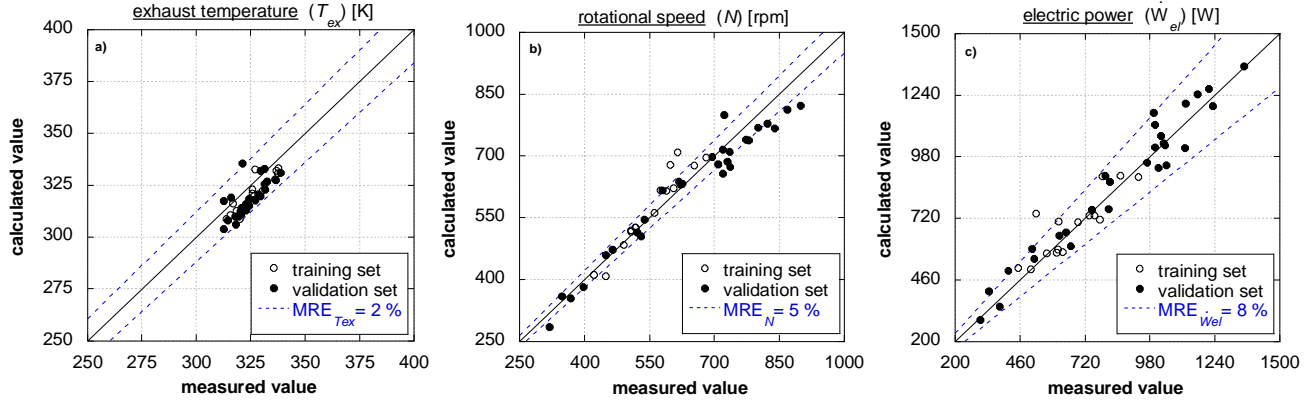


Figure 10. Parity plots of exhaust temperature a), rotational speed b) and electric power c) – lumped parameters model.

Table 6. Errors obtained by the validation process.

	"polynomial fitting functions model"	"lumped parameters model"
$MRE_{Tex}$	2.2 %	<b>1.0 %</b>
$MRE_N$	<b>4.6 %</b>	9.6 %
$MRE_{Wel}$	7.7 %	<b>4.3 %</b>
$GEF_{val}$	5.0 %	<b>4.8 %</b>

#### 4.1 Performance prediction maps

The above described calibrated models can be used to predict the performance maps of the volumetric expander out of the explored range of operating conditions. To this purpose, the extrapolation capability of the two models is shown and compared in Figures 11-14.

In details, Figure 11 focuses on the electric power output results as function of the organic fluid mass flow rate.

Figure 12 shows and compares results of electric isentropic efficiency ( $\eta_{is,el}$ ), defined in Eq. (43), as function of the pressure ratio:

$$\eta_{is,el} = \dot{W}_{el} / \dot{W}_{is} \quad (43)$$

The expander rotational speed results are shown in Figure 13. Finally, the filling factors ( $FF$ ) values, defined as in Eq. (44), as one of the main parameters of interest for volumetric expanders, are plotted in Figure 14 against the pressure ratio values.

$$FF = \dot{m} \cdot 60 / (\rho_{su} \cdot V_s \cdot N) \quad (44)$$

The parametric analysis has been set as follows: organic fluid mass flow rate variable in the range 0.02-0.24 kg/s, inlet temperature at the expander between 55 °C to 95 °C, expander discharged pressure fixed at 6 bar, expander pressure ratio variable between 1.5 and 5. As mentioned in paragraph 3.1 ("Experimental setup description"), it has been observed that the supply pressure value linearly increases with the mass flow rate in the real operation of the system. Thus, in the maps construction, the supply pressure value has been set variable with the mass flow rate, according to the experimental trend line shown in Figure 6, obtained by interpolating the available experimental data. The experimental trend of the pressure ratio as function of the mass flow rate, resulting applying this assumption, is reported in Figure 11.

Within the calibration range, the semi-empirical models show similar performance results of the aforementioned output variables. Conversely, when compared outside of the calibration range, prediction maps can substantially differ.

Both models predict an almost linear increase of electric power output with the mass flow rate: best performance is achieved at 95 °C of supply temperature and 0.24 kg/s of mass flow rate.

Significant differences among prediction maps can be observed looking at the electric isentropic efficiency results: while the polynomial model shows a linear decrease of the efficiency against the pressure ratio value, the lumped approach exhibits a maximum of 40 % of  $\eta_{is,el}$  for a pressure ratio close to 1.8. It must be pointed out that no significant influence of the supply temperature values on the electric isentropic efficiency results is detected, for both modelling. The trend of the isentropic electric efficiency as function of the pressure ratio, obtained in this work, with the lumped parameters model, is the more realistic one, and it is consistent with the isentropic efficiency curve found in Dumont et Al. [26] for a swashplate piston expander. This trend is the expected one for this type of machines [26]: indeed, it exists a pressure ratio value that allows reaching the maximum efficiency; while at lower pressure ratio, the efficiency strongly decreases because of over-expansion losses; at higher pressure ratio, instead, it decreases because of under-expansion phenomenon, pressure drop and mechanical losses. The polynomial fitting functions model overestimates the isentropic electric efficiency at low values of the pressure ratio, because it does not account for over-expansion losses.

The rotational speed trends captured at different supply temperature levels look similar comparing the modelling approaches, however the polynomial model overestimates the values of the rotational speed for pressure ratio values higher than the calibration range. As consequence, the filling factor results are underestimated compared to the lumped approach, outside of the calibration range.

From the comparison it can be concluded that, in the unexplored range of operating conditions, the lumped parameters model shows higher physical soundness in predicting the behavior of the volumetric expander compared to the polynomial fitting model.

Thus, the lumped approach can be regarded as a very useful tool for mapping the performance of the machine in a comprehensive system simulation model or for the design of new reciprocating piston expanders in specific operating conditions.

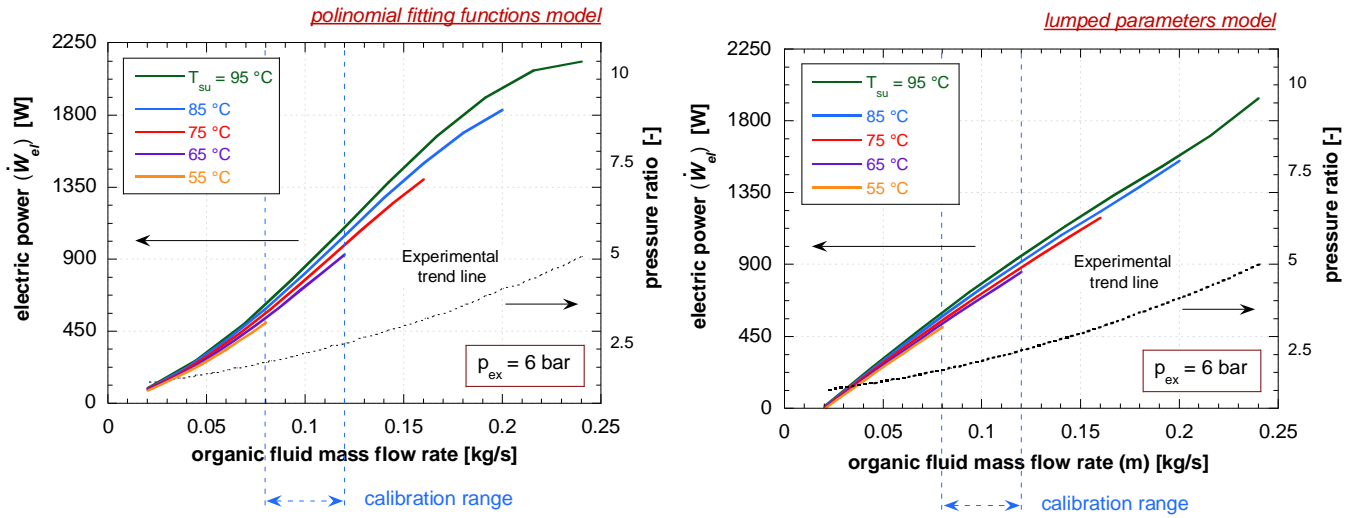


Figure 11. Prediction maps of electric power as function of the mass flow rate for different values of the supply temperature.

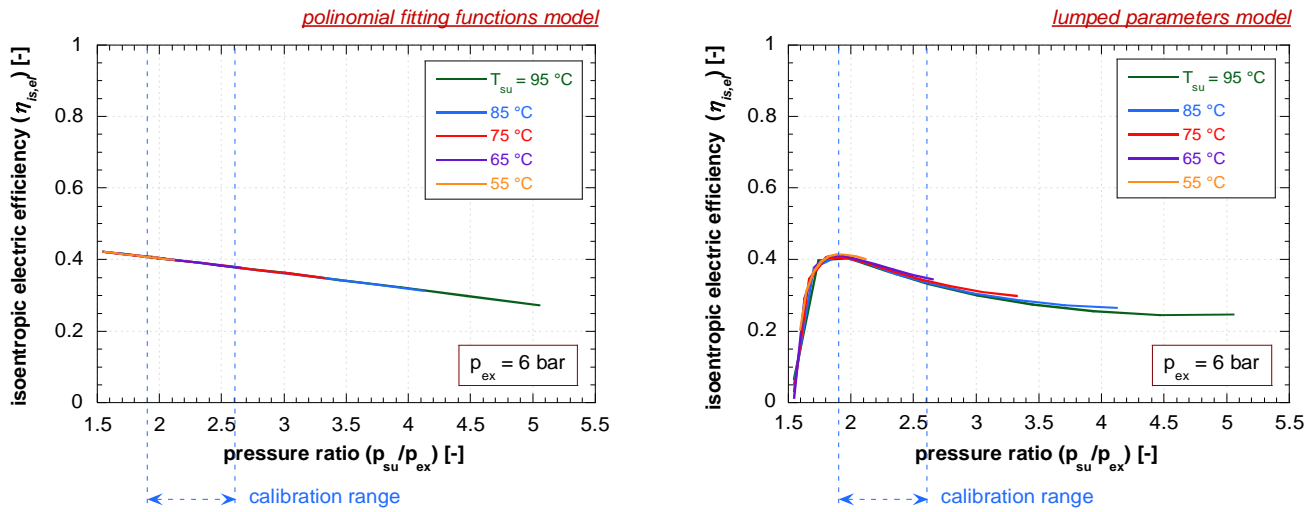


Figure 12. Prediction maps of electric isentropic efficiency as function of pressure ratio for different values of the supply temperature.

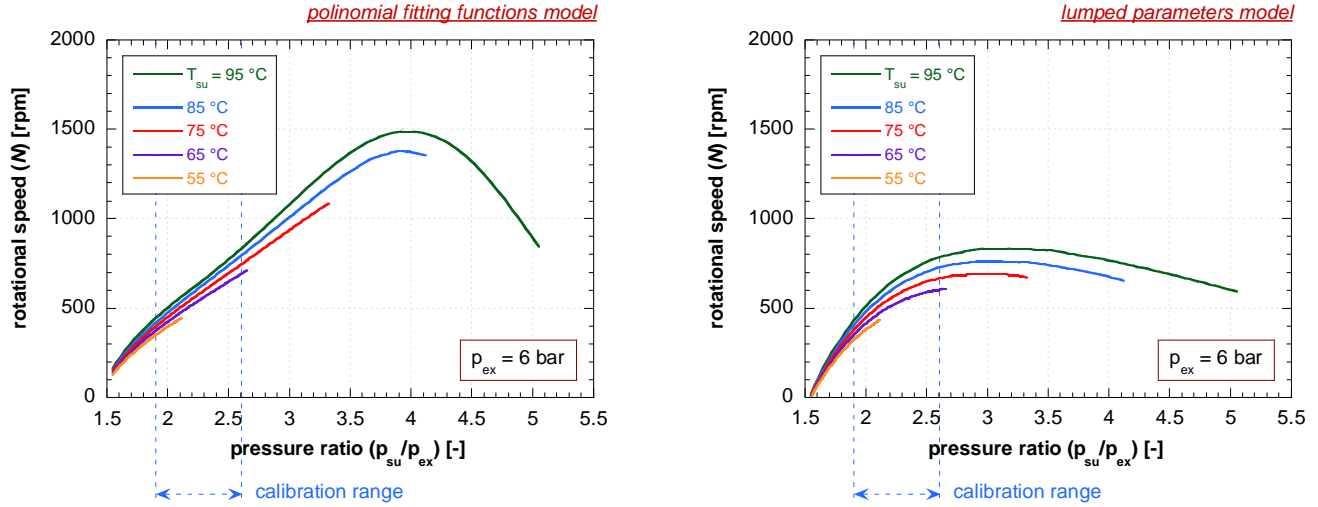


Figure 13. Prediction maps of rotational speed as function of pressure ratio for different values of the supply temperature.

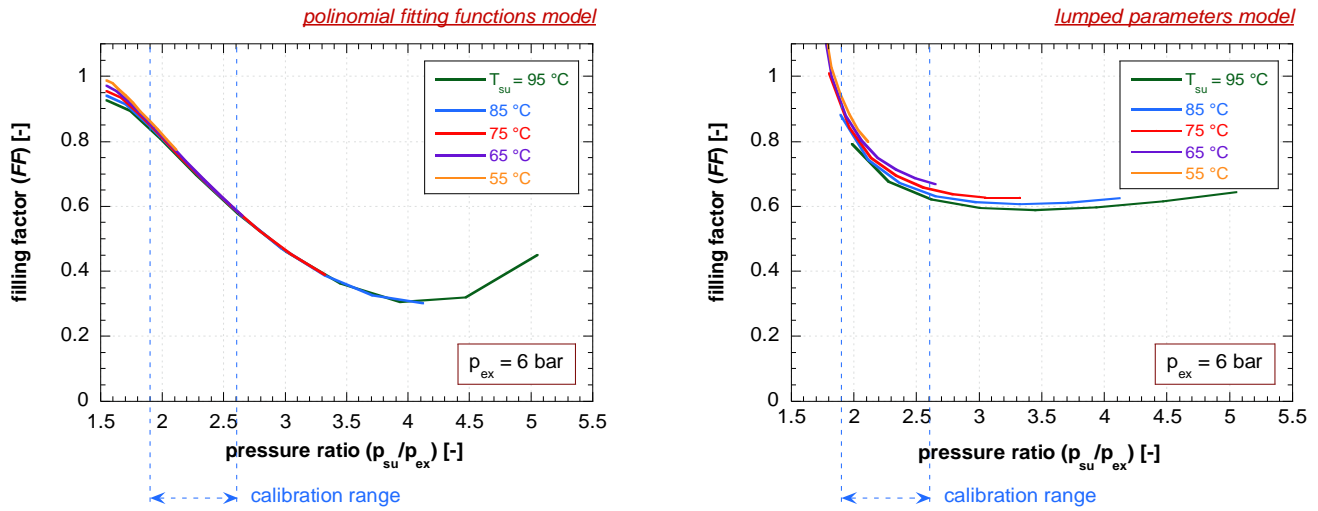


Figure 14. Prediction maps of filling factor as function of pressure ratio for different values of the supply temperature.

## 5 Conclusions

Two different semi-empirical models, originally proposed in the open literature, have been adapted and applied to a kW-size reciprocating piston expander. The selected models are characterized by different approaches: one is based on polynomial correlations to represent the expander isentropic and volumetric efficiencies (named “polynomial fitting function”); the second one accounts for key geometrical data of the expander, introducing physical equations to describe the expansion process (named “lumped parameters”).

The models have been calibrated and validated over an extensive experimental campaign carried out on a micro-scale ORC test bench for low grade heat recovery applications, where the prototype piston expander is integrated.

The calibrated models showed the lowest mean relative error values on the prediction of expander exhaust temperature (lower than 2 %). Maximum relative errors are obtained in the prediction of rotational speed for the polynomial fitting model (equal to 10 %), and in the electric power output for the lumped approach (equal to 8 %). The global mean relative error, obtained over the validation data set, is close to 5 % for both the modelling approaches.

The ability to predict the piston expander behavior in an unexplored range of operating conditions have been investigated and compared too. Results highlight that, when compared outside of the calibration range, prediction maps can substantially differ. In particular, the polynomial model shows a linear decrease of the electric isentropic efficiency against the pressure ratio. Conversely, the lumped approach exhibits a maximum of electric isentropic efficiency, equal to 40 %, at a pressure ratio of approximately 3.5.

for a pressure ratio close to 1.8 while over-expansion and under-expansion phenomena are responsible for a penalization of the efficiency values respectively at low and high pressure ratio values.

The rotational speed trends, captured at different supply temperature levels, look similar; however the polynomial model overestimates the values of the rotational speed for pressure ratio values higher than the calibration range. As consequence, the filling factor results are underestimated compared to the lumped approach. Thus, in the unexplored range of operating conditions, the lumped parameters model showed higher accuracy in predicting the behavior of the volumetric expander compared to the polynomial fitting model.



## References

- [1] Bianchi M., De Pascale A. Bottoming cycles for electric energy generation: Parametric investigation of available and innovative solutions for the exploitation of low and medium temperature heat sources. *Applied Energy* 88 (2011) 1500–1509, doi: 10.1016/j.apenergy.2010.11.013.
- [2] Pereira J. S., José B. Ribeiro J.B., Mendes R., Vaz G. C., André J. C. ORC based micro-cogeneration systems for residential application – A state of the art review and current challenges. *Renewable and Sustainable Energy Reviews* 92 (2018) 728–743, doi: 10.1016/j.rser.2018.04.039.
- [3] Lemort V., Legros A. Positive displacement expanders for Organic Rankine Cycle systems. In book: *Organic Rankine Cycle (ORC) Power Systems*.
- [4] Quoilin S., Lemort V., Lebrun J. Experimental study and modeling of an Organic Rankine Cycle using scroll expander. *Applied Energy*, vol. 87, issue 4 (2010) 1260–1268, doi: 10.1016/j.apenergy.2009.06.026.
- [5] Ziviani D., Gusev S., Lecompte S., Groll E.A., Braun J.E., Horton W.T., Van den Broek M., De Paepe M. Characterizing the performance of a single-screw expander in a small-scale organic Rankine cycle for waste heat recovery. *Applied Energy*, 181 (2016) 155–170, doi:10.1016/j.apenergy.2016.08.048.
- [6] Quoilin S., Van Den Broek M., Declaye S., Dewallef P., Lemort V. Techno-economic survey of Organic Rankine Cycle (ORC) systems. *Renewable and Sustainable Energy Reviews*, 22 (2013) 168–186, doi:10.1016/j.rser.2013.01.028.
- [7] Li W. Simplified steady-state modeling for hermetic compressors with focus on extrapolation. *International Journal of Refrigeration* 35 (2012) 1722–1733, doi:10.1016/j.ijrefrig.2012.03.008.
- [8] Molinaroli L., Joppolo C.M., De Antonellis S. A semi-empirical model for hermetic rolling piston compressors. *International Journal of Refrigeration* 79 (2017) 226–237, doi:10.1016/j.ijrefrig.2017.04.015.
- [9] D’Amico F., Pallis P., Leontaritis A.D., Karellas S., Kakalis N.M., Rech S., Lazzaretto A. Semi-empirical model of a multi-diaphragm pump in an Organic Rankine Cycle (ORC) experimental unit. *Energy* 143 (2018) 1056–1071, doi: 10.1016/j.energy.2017.10.127.
- [10] Lemort V., Quoilin S., Cuevas C., Lebrun J. Testing and modelling scroll expander integrated into an organic Rankine cycle. *Applied Thermal Engineering* 29 (2009) 3094–3102, doi: 10.1016/j.applthermaleng.2009.04.013.
- [11] Ziviani D., James N. A., Accorsi F. A., Braun J. E., Groll. E. A. Experimental and numerical analyses of a 5 kWe oil-free open drive scroll expander for small-scale organic Rankine cycle (ORC) applications. *Applied Energy* 230 (2018) 1140–1156, doi: 10.1016/j.apenergy.2018.09.025.
- [12] Mendoza L.C., Navarro-Esbri J., Bruno J.C., Lemort V., Conas A. Characterization and modeling of a scroll expander with air and ammonia as working fluid. *Applied Thermal Engineering* 70 (2014) 630–640, doi: 10.1016/j.applthermaleng.2014.05.069.
- [13] Giuffrida A. Modelling the performance of a scroll expander for small organic Rankine cycles when changing the working fluid. *Applied Thermal Engineering* 70 (2014) 1040–1049, doi: 10.1016/j.applthermaleng.2014.06.004.
- [14] Ayachi F., Ksayer E.B., Neveu P., Zoughaib A. Experimental investigation and modeling of a hermetic scroll expander. *Applied Energy* 181 (2016) 256–267, doi:10.1016/j.apenergy.2016.08.030.
- [15] Giuffrida A. Improving the semi-empirical modelling of a single screw expander for small organic Rankine cycles. *Applied Energy* 193 (2017) 356–368, doi: 10.1016/j.apenergy.2017.02.015.
- [16] Vodicka V., Novotny V., Mascuch J., Jolovratnik M. Impact of major leakages on characteristics of a rotatory vane expander for ORC. *Energy Procedia* 129 (2017) 387–394, doi: 10.1016/j.egypro.2017.09.249.
- [17] Glavatskaya Y., Podevin P., Lemort V., Shonda O., Descombes G. Reciprocating Expander for an Exhaust Heat Recovery Rankine Cycle for a Passenger Car Application. *Energies* 5 (2012) 1751–1765, ISSN 1996-1073.
- [18] Bouvier J.-L., Michaux G., Salagnac P., Kientz T., Rochier D. Experimental study of an oil -free steam piston expander for micro-combined heat and power system. *Applied Energy* 169 (2016) 788–798, doi:10.1016/j.apenergy.2018.01.049.
- [19] Bianchi M., Branchini L., Cesari N., De Pascale A., Melino F., Ottaviano S., Pinelli M., Spina P.R., Suman A. Experimental analysis of a mirco-ORC driven by piston expander for low-grade heat recovery. *Applied Thermal Engineering* 148 (2019) 1278–1291, doi: 10.1016/j.applthermaleng.2018.12.019.
- [20] Zampieri, Patent Application Publication No. US 2016/0032786 A1, United States, Feb. 4, 2016.
- [21] Bianchi M., Branchini L., De Pascale A., Orlandini V., Ottaviano S., Pinelli M., Spina P.R., Suman A. Experimental Performance of a Micro-ORC Energy System for Low Grade Heat Recovery. *Energy Procedia* 129 (2017) 899–906, doi: 10.1016/j.egypro.2017.09.096.

- 1  
2  
3  
4 [22] W. M. Kays. Convective Heat Transfer and Mass Transfer. Mc Graw-Hill, New York 1966.  
5 [23] MATLAB and Statistics Toolbox Realease 2017b, The MathWorks, Inc., Natick, Massachusetts, United States.  
6 [24] Bell I.H., Wronski J., Quoilin S., Lemort V. Pure and pseudo-pure fluid thermophysical property evaluation and the  
7 open-source thermophysical property library CoolProp. Ind. Eng. Chem. Res. 2014; vol. 53, issue 6, pp. 249-508.  
8 [25] MathWorks Documentation: <https://www.mathworks.com/help/gads/genetic-algorithm.html#>  
9 [26] Dumont O., Parthoens A., Dickes R., Lemort V. Experimental investigation and optimal performance assessment of  
10 four volumetric expanders (scroll, screw, piston and roots) tested in a small-scale organic Rankine cycle system.  
11 Energy 165 (2018) 1119-1127 doi: 10.1016/j.energy.2018.06.182.  
12  
13  
14  
15  
16  
17  
18  
19  
20  
21  
22  
23  
24  
25  
26  
27  
28  
29  
30  
31  
32  
33  
34  
35  
36  
37  
38  
39  
40  
41  
42  
43  
44  
45  
46  
47  
48  
49  
50  
51  
52  
53  
54  
55  
56  
57  
58  
59  
60  
61  
62  
63  
64  
65